Published in final edited form as:
J Cell Physiol. 2009 February ; 218(2): 385–393. doi:10.1002/jcp.21610.

Regulation of Kir2.1 channels by the Rho-GTPase, Rac1

Stephanie B. Boyer[1,2,3], **Paul A. Slesinger**[1,2], and **S.V. Penelope Jones**[2,3]

[1]Peptide Biology Laboratory, The Salk Institute for Biological Studies. La Jolla, CA 92037

[2]Neuroscience Graduate Program, University of California, San Diego, La Jolla, California 92093-0603

[3]Department of Psychiatry, School of Medicine, University of California, San Diego, La Jolla, California 92093-0603

Abstract

Mutations in Kir2.1 inwardly rectifying potassium channels are associated with Andersen Syndrome, a disease characterized by potentially fatal cardiac arrhythmias. While several Andersen-associated mutations affect membrane expression, the cytoplasmic signals that regulate Kir2.1 trafficking are poorly understood. Here, we investigated whether the Rho-family of small GTPases regulates trafficking of Kir2.1 channels expressed in HEK-293 cells. Treatment with *C. difficile* toxin B, an inhibitor of Rho-family GTPases, or co-expression of the dominant-negative mutant of Rac1 ($Rac1_{DN}$) increased Kir2.1 current density ~2-fold. However, the dominant-negative forms of other Rho-family GTPases, RhoA or Cdc42, did not alter Kir2.1 currents, suggesting a selective effect of Rac1 on Kir2.1 current density. Single-channel properties (γ, τ_o, τ_c) and total protein levels of Kir2.1 were unchanged with co-expression of $Rac1_{DN}$; however, studies using TIRF microscopy and CFP-tagged Kir2.1 revealed increased channel surface expression. Immunohistochemical detection of extracellularly-tagged HA-Kir2.1 channels showed that $Rac1_{DN}$ reduced channel internalization when co-expressed. Finally, the dominant-negative mutant of dynamin, which interferes with endocytosis, occluded the $Rac1_{DN}$–induced potentiation of Kir2.1 currents. These data suggest that inhibition of Rac1 increases Kir2.1 surface expression by interfering with endocytosis, likely via a dynamin-dependent pathway. Surprisingly, $Rac1_{DN}$ did not alter Kir2.2 current density or internalization, suggesting subunit specific modulation of Kir2.1 channels. Consistent with this, construction of Kir2.1/2.2 chimeras implicated the C-terminal domain of Kir2.1 in mediating the potentiating effect of $Rac1_{DN}$. This novel pathway for regulating surface expression of cardiac Kir2.1 channels could have implications for normal and diseased cardiac states.

Keywords

Kir2; GTPase; Endocytosis

INTRODUCTION

Inwardly rectifying potassium channels, and Kir2 channels in particular, are crucial for setting a sharp threshold for excitation in excitable cells, as well as stabilizing the resting membrane potential in both excitable and non-excitable cells. Because of these properties, Kir2 channels regulate a variety of physiological processes, including heart rate, neuronal firing patterns, vascular smooth muscle tone, hormone secretion and activation of immune responses. They

Address Correspondence to: Stephanie B. Boyer Peptide Biology Lab Salk Institute for Biological Studies 10010 N. Torrey Pines La Jolla, CA 92037 Tel. (858) 454-4100x1681 Fax (858) 552-1546 sboyer@ucsd.edu or slesinger@salk.edu.

are particularly important in cardiac cells where they underlie I_{K1}, the cardiac inwardly rectifying potassium conductance, and play a crucial role in shaping the action potential. Kir2.1 knockout mice die shortly after birth; however, studies in neonates reveal a lack of I_{K1} current, broadened action potentials and ineffective clamping of the resting membrane potential leading to spontaneous action potentials (Zaritsky *et al*, 2001). Kir2.2 knockout mice show a 50% reduction in I_{K1}, supporting the idea that heteromers of Kir2 channels comprise native I_{K1} (Zaritsky *et al*, 2001).

Variations in Kir2 function have been implicated in a number of cardiac diseases. Reductions in Kir2.1 have been linked to hypertrophy (McIntosh *et al*, 1998), while gain-of-function mutations are associated with atrial fibrillation (Xia *et al.*, 2005) and short QT Syndrome (Priori *et al.*, 2005). Furthermore, Andersen syndrome is an autosomal dominant disorder caused by mutations in the gene encoding Kir2.1 that leads to periodic paralysis, dysmorphic features and cardiac arrhythmias (Plaster *et al.*, 2001). Studies in heterologous cells have shown that such mutations act by exerting a dominant-negative effect on mutated Kir2.1-containing heteromers (Plaster *et* al, 2001; Preisig-Muller *et al*, 2002). Recent work suggests that this may be due in part to changes in PIP_2 affinity (Lopes *et al*, 2002) and/or defects in Kir2.1 trafficking (Bendahhou *et al*, 2003).

The Kir2 family consists of four subunits, the first three of which (Kir2.1-2.3) share a high degree of homology and can form functional homo- or hetero-meric tetramers. Kir2.1-2.3 subunits also share several trafficking motifs. For instance, all three subunits share an ER-export motif (Ma *et al.*, 2001), as well as conserved residues involved in Golgi export (Stockklausner and Klocker, 2003) and putatively involved in endocytosis (Tong *et al.*, 2001). Kir2 channels also contain PDZ binding motifs, and interact with a number of PDZ domain-containing scaffolding proteins that could affect trafficking and channel stabilization in the plasma membrane (Leonoudakis *et al*, 2004). However, the cytoplasmic signals that regulate Kir2 trafficking remain largely unknown.

One candidate family of proteins that might regulate Kir2 trafficking are the small G proteins, the Rho family GTPases. Rho GTPases act as signal transducers for a variety of cellular processes and have been well studied in cardiac cells as players in hypertrophy and heart failure (reviewed by Brown *et al*, 2006). Of the Rho family, Rho, Rac and Cdc42 are the most fully characterized. They have recently been implicated in channel trafficking. Bezzerides *et al.* (2004) revealed that Rac1 is required for rapid vesicular insertion of the TRPC5 cation channel into the plasma membrane, while other evidence points to a role for Rac in internalization (Lamaze *et al.*, 2001). Furthermore, Kv1.2, a delayed rectifier potassium current, is inhibited by tyrosine kinase phosphorylation in a Rho-dependent manner (Cachero *et al.*, 1998). Stimulation of m1-muscarinic receptors leads to inhibition of Kir2.1 via RhoA (Jones, 2003), although the exact mechanism remains unresolved. Here, we examined whether RhoGTPases could regulate trafficking of I_{K1} channels (Kir2).

MATERIALS AND METHODS

Cell culture and transfection procedures

tsA201 (also known as human embryonic kidney (HEK) 293T) cells were grown in Dulbecco's modified Eagle's medium supplemented with 10% fetal calf serum, and incubated at 37°C in 5% CO_2. Cells were transiently transfected with two or more cDNAs using Lipofectamine 2000 (Invitrogen, Carlsbad, CA). Control cells were co-transfected with Kir2.1 cDNA and either β-galactosidase (β-gal) or empty pcDNA3 vector, while test cells were co-transfected with the Kir2.1 and small G-protein cDNAs, at a ratio of 1:1. For occlusion experiments, cells were transfected with Kir2.1 and each of two small G-protein cDNAs at a ratio of 1:1:1; control cells were transfected with Kir2.1 and the control plasmid at 1:2 to obtain the same total amount

of cDNA transfected. Experiments were performed 48 hours following transfection. Previous experiments have indicated a high degree (>90%) of co-transfection with the methods used here. Several separate transfections were performed for each set of conditions. Control and test transfections were performed in pairs and the experiments were interleaved. For experiments using *C. difficile* toxin B (Calbiochem, San Diego, CA), 100 pg/mL toxin B was diluted in DMSO and added to cells transfected with Kir2.1 and β-gal for 3 or 6 hours at 37°C prior to electrophysiological recording. DMSO alone was used as a vehicle control (VEH).

DNA Constructs

Kir2.1, kindly provided by Dr. L.Y. Jan (Kubo *et al*., 1993), has been inserted into the vector pcDNA3 (Invitrogen, Carlsbad, CA) as reported previously (Jones, 1996). Kir2.2 and Kir2.3 were kind gifts from Dr. Kurachi (Morishige *et al.*, 1994; Takahashi *et al.*, 1994) and were inserted into pcDNA3 as described previously (Rossignol and Jones, 2005). Dr. S. Schmid generously donated the dominant negative dynamin-1 mutant (Dyn_1K44A, Dyn_{DN}) (Hinshaw and Schmid, 1995). The mutant forms of the RhoGTPases were generous gifts from Dr. J.S. Gutkind (Coso *et al.*, 1995). The constitutively active mutants were generated by replacing glutamine for leucine by PCR-directed mutagenesis in a position analogous to that of codon 61 of Ras, generating $Rac1_{QL}$ at codon 61 as described by Coso *et al.* (1995). Such a mutation has been shown to inhibit the GTPase activity of these proteins resulting in a constitutively active protein. The dominant negative mutants of the small G-proteins were synthesized by replacement of the amino acid threonine for asparagine in a position analogous to codon 17 of Ras, generating Rac1N17 ($Rac1_{DN}$), Cdc42N17 ($Cdc42_{DN}$) and RhoAN19 ($RhoA_{DN}$). These inhibitory mutants act as antagonists by competitively inhibiting the interaction of endogenous G-proteins with their respective guanine nucleotide exchange factors (GEFs) and blocking transduction of the signal. Kir2.1 tagged with eCFP at the Kir2.1 N-terminal domain was created by inserting Kir2.1 into peCFP-N1 modified to contain the Cerulean CFP variant (Clontech) between BamHI and PstI. Chimeric channels were generously provided by Dr. A. Collins (Collins *et al.*, 2005) and Dr. L.Y. Jan (Tinker *et al.*, 1996), and were subcloned into pcDNA3.1. HA-Kir2.1-AAA was made by inserting an HA tag in the extracellular region (between aa 115 & 116) and mutating the selectivity filter from GYG to AAA, in pcDNA3.1. HA-Kir2.2 containing an HA tag in the extracellular region (between aa 115 & 116) was a kind gift from Dr. Y. Nakajima (Chen *et al*, 2002) and was subcloned into pcDNA3.1. For total internal reflection fluorescence (TIRF) experiments, cells were plated on 35mm glass bottom culture dishes (MatTek) coated with rat tail collagen and poly-D-lysine.

Electrophysiological recordings

Kir2.1 whole-cell currents were recorded using a List EPC-7 patch clamp amplifier, as described previously (Jones, 1996). All experiments were carried out at room temperature. Electrodes were pulled on a three stage horizontal puller (Mecanex, Basel, Switzerland) to yield resistances of 4-8 MΩs. Currents were low-pass filtered at 1 kHz with an 8-pole Bessel filter, digitized through an ITC-16 analog-digital converter (Instrutech, Port Washington, NY) and sampled at 2 kHz with a Macintosh Quadra 800 computer. Currents were acquired with Axodata (Axon Instruments, Union City, CA). Cellular capacitance was determined by integration of the capacitative transient elicited by a 2 mV step. Control capacitance was 27 ± 2 pF (n=35) and remained constant throughout the study with the exception of Dyn_{DN}-transfected cells which displayed an average capacitance of 20 ± 1 pF (n=21). Series resistance was generally low (around 12 MOhm) and no series resistance compensation was applied; however, voltage errors were calculated in each cell with the known Rs values and cells with errors greater than 10 mV were excluded from further analysis.

Currents were elicited by holding the cells in whole-cell voltage-clamp at a potential of -60 mV and stepping the membrane to potentials ranging from -160 to 10 mV for 200 ms in 10

mV increments as described previously (Jones, 1996; 2003). This protocol was repeated every 2 minutes for the duration of the experiment. After initial breakthrough into the whole cell mode, a 10-minute period was allowed for stabilization of the current amplitude prior to final current measurements. Transfection was assayed by the presence of an inwardly rectifying current with reversal at Ek. Previous experiments have indicated a high degree of co-transfection with the methods used here.

Single-channel recordings were performed using the cell-attached patch configuration. Electrodes were coated with Sylgard^{TN} and fire polished. Recordings were performed in high potassium solution to force the resting membrane potential toward 0 mV. Spontaneous channel activity was monitored at potentials ranging from 0 to -120 mV, for 30 s to several minutes. Currents were sampled at 5 kHz and subsequently low-pass filtered offline at 500 Hz using a Bessel 8-pole filter.

Currents were analyzed off-line, using Axograph software and P-Clamp 9.0 (Axon Instruments). For whole-cell currents, measurements were determined by averaging the last 10 data points of the 200 ms step. Current amplitudes were divided by cellular capacitance to account for differences in cell size and are reported as current density (pA/pF). Single-channel characteristics such as single channel amplitude, probability of opening and open and closed dwell times were analyzed using P-Clamp. Linear fits were made to I-V plots using at least three data points per cell to calculate slope conductance. Statistical significance was determined using non-parametric statistical methods. Data are presented as the mean ± the standard error.

Recording solutions

The extracellular recording solution was composed of (in mM): 150 NaCl, 5 KCl, 2 CaCl2, 1 MgCl2, 5 HEPES, 20 glucose. The pH was adjusted to 7.4 and the osmolarity was adjusted to 325-330 mmol/kg. The intracellular patch pipette solution contained (in mM): 150 K-gluconate, 2 MgCl2, 1.1 EGTA, 0.1 CaCl2, 5 HEPES, 5 Mg-ATP, 0.1 Li-GTP. The pH was adjusted to 7.2 and the osmolarity to 315-320 mmol/kg. Single-channel recordings were performed in symmetrical, high potassium solution consisting of (in mM): 150 KCl, 2 CaCl2, 1 MgCl2, 5 HEPES, 25 glucose. The pH was adjusted to 7.4 and the osmolarity to 320-330 mmol/kg.

Western Blotting

For analysis of total Kir2.1 expression, cells were grown on 10cm culture dishes and transfected with HA-Kir2.1 and empty pcDNA3 vector (control) or $Rac1_{DN}$ as described above. 48 hours post transfection, cells were washed 3X in PBS+ (containing calcium and magnesium; Invitrogen), scraped and homogenized with an 18G syringe needle and incubated for 1 hour on ice in lysis buffer. Protein levels were quantified using BCA Protein Assay Reagent (Pierce). 30 ug total protein was run on an SDS-PAGE gel, transferred to nitrocellulose membrane and blocked 1 hour in 5% milk in Tris-buffered saline (TBST). Membranes were incubated in mouse anti-HA primary antibody (1:500; Covance) followed by goat anti-mouse HRP conjugated secondary (Santa Cruz) for 1 hour each and visualized with ECL solution (Pierce) using XX film. Cells were then stripped with Restore Western Blot Stripping Buffer (Pierce), blocked O/N at 4° C, and incubated with pan-actin antibody (Santa Cruz Biotechnology) followed by chicken anti-goat secondary (Santa Cruz) as a control). Optical density measurements were made using NIH ImageJ software.

Total Internal Reflection Fluorescence (TIRF) Microscopy

TIRF microscopy was used to analyze surface expression of CFP-tagged Kir2.1. Through-the-objective TIRF microscopy occurs when collimated laser light is offset to illuminate the back focal plane of the objective, which causes the laser light to arrive at the coverslip at an angle.

When this angle is greater than the critical angle (θ), an evanescent wave of excitation light is produced at the interface between two media having different refractive indices, the glass coverslip and media/cell membrane (Axelrod *et al*., 1983). The intensity of this evanescent wave falls off exponentially with distance above the interface, allowing selective imaging within ~100nm of the glass/medium interface (i.e. plasma membrane and sub-membrane regions). A Nikon TE2000 microscope was equipped with a 60x oil-immersion TIRF objective (Nikon; 1.45 NA) and a solid state DPSS 442nm laser (Melles Griot – model: 85 BTL 010), which could be adjusted manually for epifluorescence and TIRF. The TIRF angle was adjusted using a fixed point on the back focal plane. The Nikon filter cube contained a polychroic mirror with reflection bands at 440nm and 510nm, and band-passes at 475/30nm and 560/60nm (z442/514rpc; Chroma technologies). No excitation filter was used. A CFP emission filter (470/30) was placed in a filter wheel (Sutter Instruments) and controlled by a Lambda 10-2 controller (Sutter Instruments). Images (12 bit) were acquired with a 12.5 MHz Imago CCD camera (Till Photonics). The camera, laser shutters and filter wheel were electronically controlled by TILLvisION 4.0 software. Transfected cells were imaged first using epifluorescence (100 ms exposure time) and, after adjusting the laser, using TIRF (500 ms exposure) microscopy. Fluorescent intensity was analyzed using NIH ImageJ software. Background was first subtracted, then a region of interest (ROI) was drawn around the entire cell (epi) or the footprint (TIRF), and the average fluorescent intensity (in arbitrary units) was measured.

Endocytosis Assay

Cells were transfected with Kir2.1 or Kir2.2 containing an HA tag in the extracellular region and an empty pcDNA3 plasmid (Ctrl) or $Rac1_{DN}$ as described above. 48 hours post transfection cells were washed 3X in progressively colder PBS+. Cells were incubated for 15 minutes on ice with anti-HA at 1:500 (Covance). After washing in PBS, cells were returned to the 37° incubator for 0, 60 or 120 minutes. Cells were fixed in 2% PFA with 4% sucrose for 15 minutes at room temperature. After washing in PBS, cells were incubated with goat anti-mouse Alexa 647 secondary antibody (Invitrogen) for 1 hour at RT to label surface channels. Following washing and permeabilization in 0.25% TritonX-100 in PBS for 15 minutes at RT, cells were incubated with donkey anti-mouse Alexa 488 conjugated secondary antibody (Invitrogen) for 1 hour at room temperature to label the internalized pool of channels. Coverslips were mounted with Prolong Gold anti-fade reagent (Invitrogen) and imaged on a Zeiss LSM 5 Pascal Axiovert 200 confocal microscope with a Plan-Apochromat 63x/1.4 oil objective. Images were processed using NIH ImageJ software. After thresholding, an ROI was drawn around the cell and the mean intensity for each channel was measured.

RESULTS

Involvement of Rho-family GTPase Rac1 in regulating Kir2.1 channels

To investigate the putative involvement of the Rho-family of small GTPases (including Rho, Rac and Cdc42) in the regulation of Kir2.1 channels, we first utilized the bacterial cytotoxin *C. difficile* toxin B, which inhibits members of the Rho family (Just *et al*., 1995). HEK-293 cells transfected with Kir2.1 cDNA displayed strong, inwardly rectifying currents (Figs. 1A and 1B). Kir2.1-transfected cells incubated with 100 pg/mL *C. difficile* toxin B (for ≥ 6 h) displayed a significant increase in Kir2.1 current density (Figs. 1A & 1B) compared to cells incubated with vehicle alone. At -100 mV, the current density increased to 202 ± 18% of control, from -13 ± 3 pA/pF (n=14) to -26 ± 5 pA/pF (n=12) in cells pretreated with toxin B. The increase in Kir2.1 current density with *C. difficile* toxin B suggests that the Rho-family of GTPases regulate Kir2.1 channels.

To investigate which Rho-family GTPase could be involved in regulating Kir2.1 channels, we took advantage of dominant-negative mutants of Rho, Rac and Cdc42 (Coso *et al*., 1995). Dominant negative versions of these proteins act as antagonists by competitively inhibiting the interaction of endogenous G-proteins with their respective guanine nucleotide exchange factors (GEFs) and blocking transduction of the signal. In Kir2.1-transfected cells, co-transfection of the dominant-negative mutant of Rac1 ($Rac1_{DN}$) significantly increased Kir2.1 current density to 223 ± 18% of control cells (Fig. 2B), from –9 ± 1 pA/pF (n=28) in control cells to -19 ± 4 pA/pF (n=11) at -100 mV in cells transfected with $Rac1_{DN}$. Activation of RhoA has been shown previously to inhibit Kir2.1 channels, while dominant-negative RhoA had no effect (Jones, 2003). Similarly, here co-expression of the dominant-negative forms of RhoA ($RhoA_{DN}$) or Cdc42 ($Cdc42_{DN}$) did not significantly alter Kir2.1 current density, suggesting a specific role for Rac1 (Fig. 2C). Interestingly, the constitutively active mutant of Rac ($Rac1_{QL}$) did not significantly alter Kir2.1 current density (-11 ± 2 pA/pF (n=12)).

Analysis of single-channel properties of Kir2.1 channels in cells coexpressing $Rac1_{DN}$

An increase in Kir2.1 current density could be caused by an increase in the number of channels in the membrane, or by a change in the single-channel properties, such as unitary conductance (*i*), open probability (P_o) or open dwell time. To investigate the latter, we used the cell-attached patch-clamp technique to compare Kir2.1 single-channels in the absence or presence of co-expressed $Rac1_{DN}$. Unitary events for Kir2.1 channels could be recorded in cell attached patches from both cell types. To determine the single-channel conductance, we measured the unitary current between -40 and -120 mV (using equimolar K^+ to zero the cell's resting membrane potential). Single-channel conductance was calculated by determining the slope of the linear fit to the single-channel current-voltage relationship (Figure 3B). Coexpression of $Rac1_{DN}$ had little effect on Kir2.1 single channel properties, with a conductance of 15 ± 1 pS (n=4) in control cells and 15 ± 3 pS (n=6) in cells expressing $Rac1_{DN}$ (Fig. 3B). We also examined the kinetics of single-channel opening and closings by measuring the open and closed dwell times at -40 mV (comparable to -100 mV in whole-cell recordings) in 30 s traces. The mean open times at -40 mV were 154 ± 77 ms in control cells and 139 ± 63 ms in $Rac1_{DN}$ transfected cells (Fig. 3D). The mean closed times were 27 ± 15 ms in control cells and 36 ± 17 ms in $Rac1_{DN}$ transfected cells (Fig. 3E). Similarly, the open probability of the channel was also not significantly different (Fig. 3C), with Po = 0.8 ± 0.1 in control and 0.8 ± 0.05 in $Rac1_{DN}$ transfected cells at -40 mV (n=5-6). Macroscopic current (I) is determined by the number of channels (N), P_o and *i* ($I = NP_oi$). Therefore, these experiments suggest that $Rac1_{DN}$ may alter the number of channels at the plasma membrane.

Inhibiting endocytosis with Dyn_{DN} occludes the potentiation effect of $Rac1_{DN}$

A change in the number of Kir2.1 channels could be caused by insertion of new Kir2.1 channels into the membrane, a reduction in endocytosis or a combination of the two. To test the effect of reduced endocytosis on Kir2.1 current density, we utilized a dominant negative form of dynamin ($Dyn1_{K44A}$ or Dyn_{DN}), which blocks the endocytic process (Hinshaw and Schmid, 1995). Co-expression of Dyn_{DN} significantly increased Kir2.1 current density (Figure 4). Expression of Dyn_{DN} increased Kir2.1 current density to 191 ± 12% of control (-9 ± 2 pA/pF for control (n=16) vs. -18 ± 2 pA/pF in Dyn_{DN} transfected cells (n=15, Fig. 4C). Thus, inhibiting a dynamin-dependent endocytic pathway increases Kir2.1 current density.

We next examined the effect of co-expressing $Rac1_{DN}$ with Dyn_{DN} on Kir2.1 currents. If $Rac1_{DN}$ promotes exocytosis while Dyn_{DN} inhibits endocytosis, we would expect to see an additive effect and an increase in Kir2.1 current. The Kir2.1 current density increased to 202 ± 13% (n=12) of control, which was not significantly different from that caused by Dyn_{DN} or $Rac1_{DN}$ alone (Fig. 2C; Fig. 4C). Thus, inhibiting endocytosis appears to occlude the effect of

$Rac1_{DN}$, suggesting that $Rac1_{DN}$ may interfere with the dynamin-dependent endocytosis of Kir2.1.

$Rac1_{DN}$ increases surface expression of Kir2.1

To independently assay whether changes in Kir2.1 current density could be attributed to changes in surface expression, we used TIRF microscopy to study the surface expression of CFP-tagged Kir2.1 channels in the absence or presence of coexpressed $Rac1_{DN}$. TIRF microscopy allows visualization of channel proteins expressed in the plasma membrane and sub-membrane regions up to ~100nm (Axelrod *et al.*, 1983; Fowler *et al.*, 2007). To visualize Kir2.1 channels, we fused cyan fluorescent protein (CFP) to the N-terminus of Kir2.1 and imaged under both wide-field epifluorescence and TIRF. CFP-Kir2.1 was detected using both wide-field and TIRF illumination. The intensity of CFP-Kir2.1 fluorescence under TIRF increased to 213 ± 18% in cells co-expressing $Rac1_{DN,}$ compared to control cells expressing CFP-Kir2.1 and a control plasmid (Fig. 5A). Similarly, inhibition of endocytosis with Dyn_{DN} increased surface fluorescence of CFP-Kir2.1 (189 ± 22% of control). By contrast, co-expression of $Rac1_{QL}$ or Rho_{DN} did not significantly alter CFP-Kir2.1 fluorescence on the plasma membrane (Fig. 5B). These changes in surface expression of CFP-Kir2.1 channels measured with TIRF are similar to the changes in current density measured with electrophysiology. Taken together, these results suggest that Rac1 modulates surface levels of Kir2.1 channel expression.

To ensure that $Rac1_{DN}$ did not alter Kir2.1 surface levels non-specifically by increasing total Kir2.1 protein expression, we performed immunoblotting of total Kir2.1 protein levels using an HA-tagged Kir2.1. Cells showed similar levels of total Kir2.1 protein expression under control and $Rac1_{DN}$-expressing conditions (Fig. 5E). Membranes were stripped and blotted for actin levels as a control (Fig. 5E). $Rac1_{DN}$ co-expression did not alter the ratio of Kir2.1 to actin protein expression compared to control cells (Fig. 5F, $p > 0.05$). This suggests that the increases in surface expression and current density of Kir2.1 upon co-expression of $Rac1_{DN}$ are not due to changes in total Kir2.1 protein levels.

Rac1 specificity for Kir2.1 over Kir2.2/2.3 channels is mediated by Kir2.1 C-terminus

Kir2.1, Kir2.2 and Kir2.3 channels share 60% or greater identity in amino acid sequence. We investigated whether Kir2.2 or Kir2.3 channels were also sensitive to regulation by Rac1. Expression of Kir2.2 or Kir2.3 cDNA yielded inwardly rectifying K^+ currents that were similar to Kir2.1 channels (Figs. 6A and 6C). Co-expression of $Rac1_{DN}$ did not significantly alter the current density of either Kir2.2 or Kir2.3 channels (Figs. 6B and 6D). Thus, the effect of Rac1 modulation appears to be specific for the Kir2.1 channel subunit.

To localize the region of the Kir2.1 channel that might mediate regulation by Rac1, we utilized Kir2.1/2.2 chimeric channels (Collins *et al.*, 2005; Tinker *et al.*, 1996), in which the N-and C-terminal domains were exchanged (Fig. 7A). Chimera 2.1_N-2.2 contains the N-terminal domain of Kir2.1 fused to Kir2.2 at amino acid 78 (Collins *et al.*, 2005) and chimera 2.2_N-2.1 contains the N-terminal and first transmembrane domain of Kir2.2 fused to Kir2.1 at amino acid 121 (Tinker *et al*, 1996). Transfection of cDNA for 2.1_N-2.2 and 2.2_N-2.1 yielded inwardly rectifying K currents, having current densities of -36.3 ± 8.3 pA/pF and -8.2 ± 2.3 pA/pF for 2.1_N-2.2 and 2.2_N-2.1, respectively.

Similar to wild-type Kir2.2, co-expression of $Rac1_{DN}$ did not change the current-voltage relationship or current density for 2.1_N-2.2 channels (Figs. 7B and 7C). By contrast, $Rac1_{DN}$ coexpression increased 2.2_N-2.1current density to 178 ± 29% (n=9) of control (Fig. 7E), without altering the current kinetics or current-voltage relationship. Taken together, these

experiments suggest that the selective effects of Rac1 are mediated by the C-terminal and/or pore domain of Kir2.1.

$Rac1_{DN}$ inhibits internalization of Kir2.1 but not Kir2.2 channels

Co-expression studies with Dyn_{DN} and Rac_{DN} together suggested that Rac1 alters Kir2.1 endocytosis in a dynamin-dependent manner (Fig.4). To investigate this further, we performed an internalization assay using Kir2.1 channels containing an extracellular HA epitope. The surface population of Kir2.1 channels were detected by incubation with anti-HA antibodies on ice for 15 minutes. Cells were then returned to the 37° C incubator for 0, 60 or 120 minutes to monitor the internalization of the channels. Cells were stained prior to permeabilization to label surface channels and subsequently permeabilized and stained with a second fluorophore to label the internalized pool of channels. At time 0, both control and $Rac1_{DN}$ expressing cells showed a high degree of surface labeling of Kir2.1 (Fig. 8A & B). By 60 minutes, control cells showed ~60% decrease in Kir2.1 surface expression and a concomitant increase in internalized Kir2.1 (Fig. 8A & E). By contrast, even after 120 minutes, cells coexpressing $Rac1_{DN}$ failed to show either a decrease in surface levels of Kir2.1 or any detectable level of internalized Kir2.1 channels (Fig. 8B & F). Similar results were obtained with cells co-expressing Kir2.1 and Dyn_{DN} (Fig. 8 C & G). Kir2.2 channels, on the hand, showed ~80% decrease in surface expression and a high degree of internalized channels at 120 minutes even with $Rac1_{DN}$ coexpression (Fig. 8D & H). These results suggest that $Rac1_{DN}$ prevents internalization of Kir2.1 channels but has no effect on Kir2.2 channels, consistent with the specificity seen with current density measurements.

DISCUSSION

In this study, we found that selective inhibition of the endogenous GTPase Rac1 increased the current density of Kir2.1 channels by nearly two-fold while the dominant-negative mutants of Cdc42 or RhoA did not significantly alter the current density. Similarly, the potentiation of current with $Rac1_{DN}$ was observed only with Kir2.1 and not the related Kir2.2 or Kir2.3 channels, indicating a high degree of specificity. Subsequent chimeric studies implicated the C-terminal domain of Kir2.1 in enabling modulation by Rac1. Several lines of evidence suggest that the potentiation of current resulted from reduced basal internalization, leading to greater Kir2.1 surface expression; (i) the intensity of CFP-tagged Kir2.1 channels increased in the plasma membrane in the presence of $Rac1_{DN}$, without affecting total protein levels, (ii) a dominant-negative mutant of dynamin, known to be involved in endocytosis, mimicked and occluded the effect of $Rac1_{DN}$, (iii) the rate of basal internalization of Kir2.1 was dramatically slowed in cells co-expressing $Rac1_{DN}$. These results suggest that Rac1 is involved in regulating the levels of Kir2.1 channels expressed on the membrane surface.

Changes in Kir2.1 current density could also be achieved through other pathways. For instance, a Rac-induced enhancement in membrane PIP_2 levels could, in theory, lead to an increase in current density. However, this explanation seems unlikely since Kir2.1 channels bind PIP_2 with high affinity and would show little change with increased levels of PIP_2 (Huang et al, 1998). Furthermore, both Kir2.1 and Kir2.2 channels bind PIP_2 with high affinity, but Rac1 modulates only Kir2.1. An increase in current density could also arise from an enhancement of Kir2.1 channels already expressed on the plasma membrane. For example, Sun et al. (2004) reported that a fraction of Kir2.1 channels on the plasma membrane appear electrically silent and these could potentially be activated by Rac1. This possibility seems unlikely because a similar magnitude increase in surface expression was measured with CFP-Kir2.1 using TIRF microscopy. Using CFP-Kir2.1 enabled us to visualize both electrically active channels and any silent channels possibly expressed in the plasma membrane. Furthermore, analysis of the rate of internalization showed that Kir2.1 channels show a high degree of constitutive

endocytosis, consistent with previous reports (Leyland & Dart, 2004). Given the established role for RhoGTPases in membrane trafficking, the most parsimonious explanation for the potentiation of Kir2.1 current is that the rate of Kir2.1 endocytosis is altered by interfering with endogenous Rac1. Consistent with this interpretation, we did not observe an additive effect of $Rac1_{DN}$ with Dyn_{DN}, suggesting $Rac1_{DN}$ acts predominantly on the internalization of Kir2.1, possibly via a dynamin-dependent mechanism.

Another possibility is that Rac1 alters the localization of Kir2.1 at the plasma membrane, possibly through lipid raft shuttling. However, Kir2.1 localizes almost exclusively to lipid rafts under normal circumstances. Furthermore, both Kir2.1 and Kir2.2 are found in lipid rafts (Romanenko *et al*, 2004), while only Kir2.1 shows regulation by Rac1. Of note, studies with interleukin 2 (IL2) receptors also found that the dominant negative mutant of Rac suppressed receptor internalization, while the activated mutant had no effect (Lamaze *et al*, 2001). IL2 receptors, like Kir2 channels, also localize to lipid rafts. This may reflect a more general role for Rac1 in a dynamin-mediated, lipid raft endocytic pathway.

Importantly, $Rac1_{DN}$ altered the current density of Kir2.1 channels but not of Kir2.2 or Kir2.3 channels, suggesting a high degree of specificity. Kir2.1-2.3 are highly homologous (60% or greater homology), including several conserved regions implicated previously in trafficking (Ma *et al*, 2001; Stockklausner & Klocker, 2003; Tong *et al*, 2001). One possibility is that Kir2.2/2.3 internalize via a mechanism fundamentally different from that of Kir2.1. Alternatively, Kir2.2/2.3 channels may lack an internalization signal required for Rac1 modulation. For example, Kir2.1 contains a dileucine motif at amino acids 231-232, which could account for the differential effects of Rac on Kir2 trafficking. Consistent with this, the chimeric channel containing the C-terminal domain and this dileucine motif of Kir2.1 did show regulation by Rac1. Because Kir2 channels form heteromeric channels, the balance of different internalization motifs will likely dictate how native, heteromeric channel complexes are regulated by Rho GTPases.

Surprisingly, the activated mutant of Rac1 did not inhibit Kir2.1 current density, as was shown previously with constitutively active RhoA (Jones, 2003). There are several possible explanations for this finding. A functional difference between RhoA and Rac1 could arise from different cellular signaling pathways. RhoA and Rac1 differ in many downstream effectors, including different scaffolding proteins, serine/threonine kinases and lipid binding proteins (Bustelo et al, 2007). It is possible that endogenous levels of Rac1 mask the effect of ectopically expressed Rac1 or the expression of ectopic Rac1 is inefficient, compared to $Rac1_{DN}$. Alternatively, $Rac1_{DN}$ may broadly suppress the activity of all subtypes of Rac, including Rac1-3, raising the possibility that Rac2 or Rac3 may enhance internalization.

The cardiac inwardly rectifying potassium conductance I_{k1} plays a crucial role in shaping the cardiac action potential, particularly during the plateau and repolarization phases. Studies in knockout mice suggest while I_{k1} is composed of both Kir2.1 and 2.2, Kir2.1 is the dominant subunit; Kir2.1 knockout mice completely lack I_{k1}, while Kir2.2 knockout mice show approximately 50% reduction in I_{k1} (Zaritsky et al, 2001). RhoGTPases are also key players in cardiac signaling, having been well studied in the context of cardiac hypertrophy. Hypertrophic agonists such as phenylephrine and endothelin-1, as well as angiotensin-II have been shown to activate Rac1, while statins block the isoprenylation and thus membrane targeting and functional activation of Rac1 in cardiac cells (Brown et al, 2006). Regulation of Kir2.1 currents by Rac could have important consequences for cardiac function. Andersen Syndrome mutations in the gene encoding Kir2.1 result in a reduction in channel function, through changes in either channel gating or trafficking (Ricardo Perez Riera *et al*, 2004). Upregulation of Kir2.1 currents leads to multiple abnormalities of cardiac excitability, including atrioventricular (AV) block and atrial fibrillation (AF) (Li *et al*, 2004). Interestingly,

transgenic mice expressing a cardiac-targeted guanine nucleotide dissociation inhibitor (GDI) that binds Rho family members (including Rho, Rac and Cdc42) in their inactive, GDP-bound forms resulted in normal ventricular conductance, but several atrial arrhythmias, including AV block in all animals and atrial fibrillation in a small percentage of animals (Wei *et al*, 2004). While the exact mechanism through which Rac regulates Kir2 trafficking remains to be determined, we speculate that Rac1 plays an important role in regulating surface levels of Kir2.1 in the heart.

LITERATURE CITED

Axelrod D, Thompson NL, Burghardt TP. Total internal inflection fluorescent microscopy. J Microsc 1983;129:19–28. [PubMed: 6827590]

Bendahhou S, Donaldson MR, Plaster NM, Tristani-Firouzi M, Fu YH, Ptácek LJ. Defective potassium channel Kir2.1 trafficking underlies Andersen-Tawil syndrome. J Biol Chem 2003;51:51779–51785. [PubMed: 14522976]

Bezzerides VJ, Ramsey IS, Kotecha S, Greka A, Clapham DE. Rapid vesicular translocation and insertion of TRP channels. Nat Cell Bio 2004;6:709–720. [PubMed: 15258588]

Brown JH, Del Re DP, Sussman MA. The Rac and Rho hall of fame: a decade of hypertrophic signaling hits. Circ Res 2006;98:730–742. [PubMed: 16574914]

Bustelo XR, Sauzeau V, Berenjeno IM. GTP-binding proteins of the Rho/Rac family: regulation, effectors and functions in vivo. Bioessays 2007;29:356–37. [PubMed: 17373658]

Cachero TG, Morielli AD, Peralta EG. The small GTP-binding protein RhoA regulates a delayed rectifier potassium channel. Cell 1998;93:1077–1085. [PubMed: 9635436]

Collins A, Wang H, Larson MK. Differential sensitivity of Kir2 inward-rectifier potassium channels to a mitochondrial uncoupler: identification of a regulatory site. Mol Pharmacol 2005;67:1214–1220. [PubMed: 15632319]

Coso OA, Chiariello M, Kalinec G, Yu J-C, Teramoto H, Crespo P, Xu N, Miki T, Gutkind JS. The small GTP-binding proteins Rac1 and Cdc42 regulate the activity of the JNK/SAPK signalling pathway. Cell 1995;81:1137–1146. [PubMed: 7600581]

Fowler CE, Aryal P, Suen KF, Slesinger PA. Evidence for association of GABA(B) receptors with Kir3 channels and regulators of G protein signalling (RGS4) proteins. J Physiol 2007;580:51–65. [PubMed: 17185339]

Hinshaw JE, Schmid SL. Dynamin self-assembles into rings suggesting a mechanism for coated vesicle budding. Nature 1995;374:190–192. [PubMed: 7877694]

Huang CL, Feng S, Hilgemann D. Direct activation of inward rectifier potassium channels by PIP_2 and its stabilization by G$\beta\gamma$. Nature 1998;391:803–806. [PubMed: 9486652]

Jones SVP. Modulation of the inwardly rectifying potassium channel IRK1 by the m1 muscarinic receptor. Mol Pharmacol 1996;49:662–667. [PubMed: 8609894]

Jones SVP. Role of the small GTPase Rho in modulation of the inwardly rectifying potassium channel Kir2.1. Mol Pharmacol 2003;64:987–993. [PubMed: 14500755]

Just, I.; Selzer, J.; Wilm, M.; von Eichel-Streiber, C.; Mann, M.; Aktories, K. Glucosylation of Rho proteins by Clostridium difficile toxin B. 1995. p. 500-503.

Kubo Y, Baldwin TJ, Jan YN, Jan LY. Primary structure and functional expression of a mouse inward rectifier potassium channel. Nature 1993;362:127–132. [PubMed: 7680768]

Lamaze C, Dujeancourt A, Baba T, Lo CG, Benmerah A, Dautry-Varsat A. Interleukin 2 receptors and detergent-resistant membrane domains define a clathrin-independent endocytic pathway. Mol Cell 2001;7:661–671. [PubMed: 11463390]

Leonoudakis D, Conti LR, Radeke CM, McGuire LM, Vandenberg CA. A multiprotein trafficking complex composed of SAP97, CASK, Veli, and Mint1 is associated with inward rectifier Kir2 potassium channels. J Biol Chem 2004;279:19051–19063. [PubMed: 14960569]

Leyland ML, Dart C. An alternatively spliced isoform of PSD-93/chapsyn 110 binds to the inwardly rectifying potassium channel, Kir2.1. J Biol Chem 2004;279:43427–43436. [PubMed: 15304517]

Li J, McLerie M, Lopatin AN. Transgenic upregulation of IK1 in the mouse heart leads to multiple abnormalities of cardiac excitability. Am J Physiol Heart Circ Physiol 2004;287:H2790–H2802. [PubMed: 15271672]

Lopes CM, Zhang H, Rohacs T, Jin T, Yang J, Logothetis DE. Alterations in conserved Kir channel-PIP2 interactions underlie channelopathies. Neuron 2002;34:933–944. [PubMed: 12086641]

Ma D, Zerangue N, Lin YF, Collins A, Yu M, Jan YN, Jan LY. Role of ER export signals in controlling surface potassium channel numbers. Science 2001;291:316–319. [PubMed: 11209084]

McIntosh MA, Cobbe SM, Kane KA, Rankin AC. Action potential prolongation and potassium currents in left-ventricular myocytes isolated from hypertrophied rabbit hearts. J Mol Cell Cardiol 1998;30:43–53. [PubMed: 9500863]

Morishige K-I, Takahashi N, Jahangir A, Yamada M, Koyama H, Zanelli JS, Kurachi Y. Molecular cloning and functional expression of a novel brain-specific inward rectfier potassium channel. FEBS Lett 1994;346:251–256. [PubMed: 8013643]

Chen L, Kawano T, Bajic S, Kaziro Y, Itoh H, Art JJ, Nakajima Y, Nakajima S. A glutamate residue at the C terminus regulates activity of inward rectifier K+ channels: implication for Andersen's syndrome. PNAS 2002;99:8430–8435. [PubMed: 12034888]

Plaster NM, Tawil R, Tristani-Firouzi M, Canun S, Bendahhou S, Tsunoda A, Donaldson MR, Iannaccone ST, Brunt E, Barohn R, Clark J, Deymeer F, George AL Jr, Fish FA, Hahn A, Nitu A, Ozdemir C, Serdaroglu P, Subramony SH, Wolfe G, Fu YH, Ptacek LJ. Mutations in Kir2.1 cause the developmental and episodic electrical phenotypes of Andersen's syndrome. Cell 2001;105:511–519. [PubMed: 11371347]

Preisig-Müller R, Schlichthörl G, Goerge T, Heinen S, Brüggemann A, Rajan S, Derst C, Veh RW, Daut J. Heteromerization of Kir2.x potassium channels contributes to the phenotype of Andersen's syndrome. Proc Natl Acad Sci USA 2002;99:7774–7779. [PubMed: 12032359]

Priori SG, Pandit SV, Rivolta I, Berenfeld O, Ronchetti E, Dhamoon A, Napolitano C, Anumonwo J, di Barletta MR, Gudapakkam S, Bosi G, Stramba-Badiale M, Jalife J. A novel form of short QT syndrome (SQT3) is caused by a mutation in the KCNJ2 gene. Circ Res 2005;96:703–704. [PubMed: 15831819]

Ricardo Pérez Riera A, Ferreira C, Dubner SJ, Schapachnik E. Andersen syndrome: the newest variant of the hereditary-familial long QT syndrome. Ann Noninvasive Electrocardiol 2004;9:175–179. [PubMed: 15084216]

Romanenko VG, Fang Y, Byfield F, Travis AJ, Vandenberg CA, Rathblat GH, Levitan I. Cholesterol sensitivity and lipid raft targeting of Kir2.1 channels. Biophys J 2004;87:3850–3861. [PubMed: 15465867]

Rossignol TM, Jones SVP. Regulation of a family of inwardly rectifying potassium channels (Kir2) by the m1 muscarinic receptor and the small GTPase Rho. Pflugers Arch 2005;452:164–174. [PubMed: 16328454]

Stockklausner C, Klocker N. Surface expression of inward rectifier potassium channels is controlled by selective Golgi export. J Biol Chem 2003;278:17000–17005. [PubMed: 12609985]

Sun H, Shikano S, Xiong Q, Li M. Function recovery after chemobleaching (FRAC): evidence for activity silent membrane receptors on cell surface. PNAS 2004;101:16964–196969. [PubMed: 15548608]

Takahashi N, Morishige K-I, Jahangir A, Yamada M, Findlay I, Koyama H, Kurachi Y. Molecular cloning and functional expression of cDNA encoding a second class of inward rectifier potassium channels in the mouse brain. J Biol Chem 1994;269:23274–23279. [PubMed: 8083233]

Tinker A, Jan YN, Jan LY. Regions responsible for the assembly of inwardly rectifying potassium channels. Cell 1996;87:857–68. [PubMed: 8945513]

Tong Y, Brandt GS, Li M, Shapovalov G, Slimko E, Karschin A, Dougherty DA, Lester HA. Tyrosine decaging leads to substantial membrane trafficking during modulation of an inward rectifier potassium channel. J Gen Physiol 2001;117:103–118. [PubMed: 11158164]

Wei L, Taffet GE, Khoury DS, Bo J, Li Y, Yatani A, Delaughter MC, Klevitsky R, Hewett TE, Robbins J, Michael LH, Schneider MD, Entman ML, Schwartz RJ. Disruption of Rho signaling results in progressive atrioventricular conduction defects while ventricular function remains preserved. FASEB J 2004;18:857–859. [PubMed: 15033930]

Xia M, Jin Q, Bendahhou S, He Y, Larroque MM, Chen Y, Zhou Q, Yang Y, Liu Y, Liu B, Zhu Q, Zhou Y, Lin J, Liang B, Li L, Dong X, Pan Z, Wang R, Wan H, Qiu W, Xu W, Eurlings P, Barhanin J, Chen Y. A Kir2.1 gain-of-function mutation underlies familial atrial fibrillation. Biophys Biochem Res Commun 2005;332:1012–1019.

Zaritsky JJ, Redell JB, Tempel BL, Schwarz TL. The consequences of disrupting cardiac inwardly rectifying K(+) current (I(K1)) as revealed by the targeted deletion of the murine Kir2.1 and Kir2.2 genes. J Physiol 2001;533:697–710. [PubMed: 11410627]

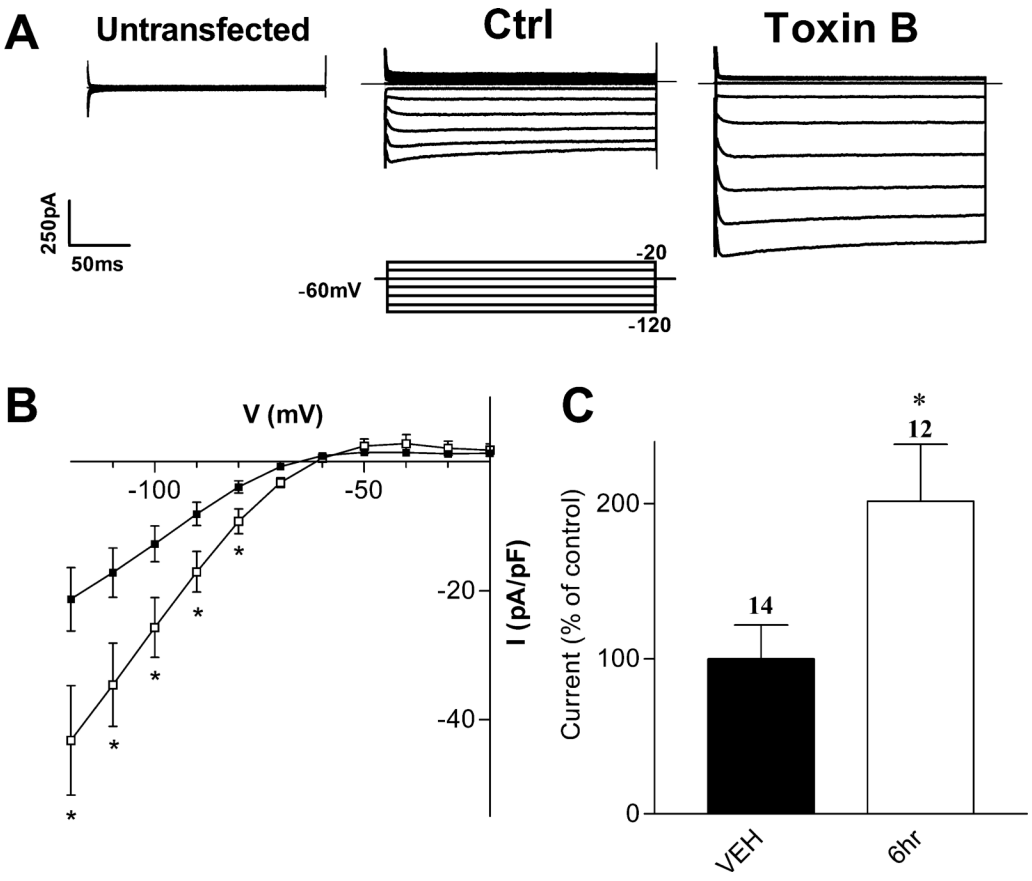

FIGURE 1. Inhibiting Rho Family GTPases Increases Kir2.1 Macroscopic Current Density

A) Representative current traces from tsA201 cells co-transfected with Kir2.1 cDNA and β-gal under control conditions or after pre-incubation with 100 pg/mL *C. difficile* toxin B. Superimposed current traces are shown for 200 ms voltage steps from -120 to -20 mV in 10 mV increments from a holding potential of -60 mV. Inset shows the voltage protocol used. *B)* Current-voltage (I-V) relationship of control cells (vehicle, filled squares) and cells incubated with toxin B for 6 hours (open squares). The currents are presented as pA/pF to compensate for potential cell size differences. *C)* Normalized current densities at –100 mV, presented as percent of control currents. Currents were normalized to the mean of control cells by day of recording. Numbers above columns indicate number of cells in each condition. Asterisks denote statistically significantly different from control cells, using non-parametric t-test ($p < 0.05$).

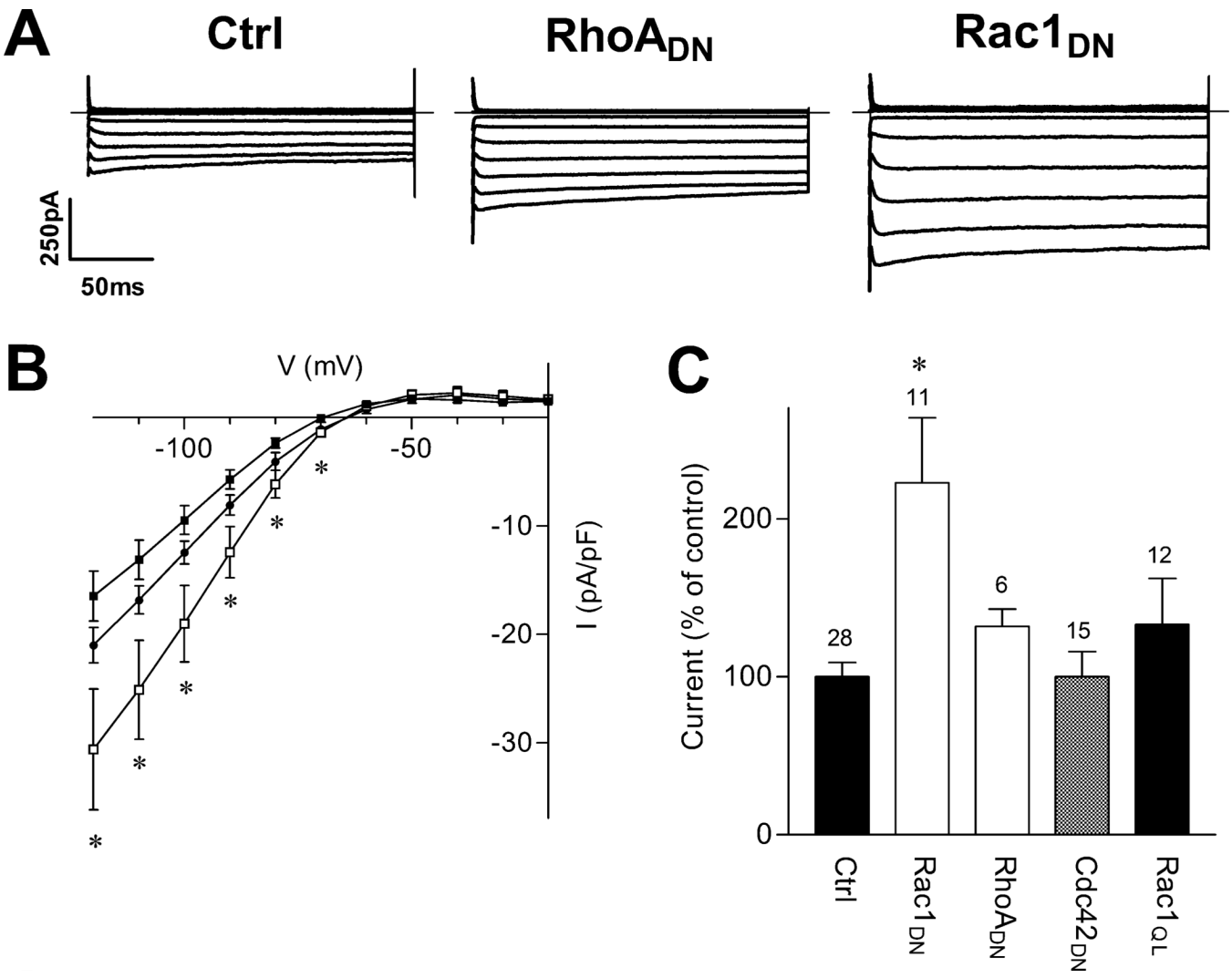

FIGURE 2. Effects of Rho Family Mutants on Kir2.1 Current Density

A) Representative current traces from tsA201 cells co-transfected with the cDNA for Kir2.1 and either a control plasmid (Ctrl), dominant-negative RhoA ($RhoA_{DN}$) or dominant-negative Rac1 ($Rac1_{DN}$) cDNA. Superimposed current traces are shown for 200 ms voltage steps from -120 to +10 mV in 10 mV increments from a holding potential of -60 mV. Scale bars: 50 ms and 250 pA. *B*) Current-voltage (I-V) relationship of control (filled squares), $Rac1_{DN}$ (open squares) and $RhoA_{DN}$ transfected cells (filled circles). *C*) Normalized current densities at –100 mV from control and mutant-GTPase transfected cells. $Cdc42_{DN}$ represents the dominant-negative mutant of Cdc42, and $Rac1_{QL}$ represents the activated mutant of Rac1. Numbers above columns indicate number of cells in each condition. Asterisks denote statistically significantly different from control cells ($p < 0.01$), using Kruskal-Wallis nonparametric ANOVA followed by Dunn's multiple comparison post hoc test.

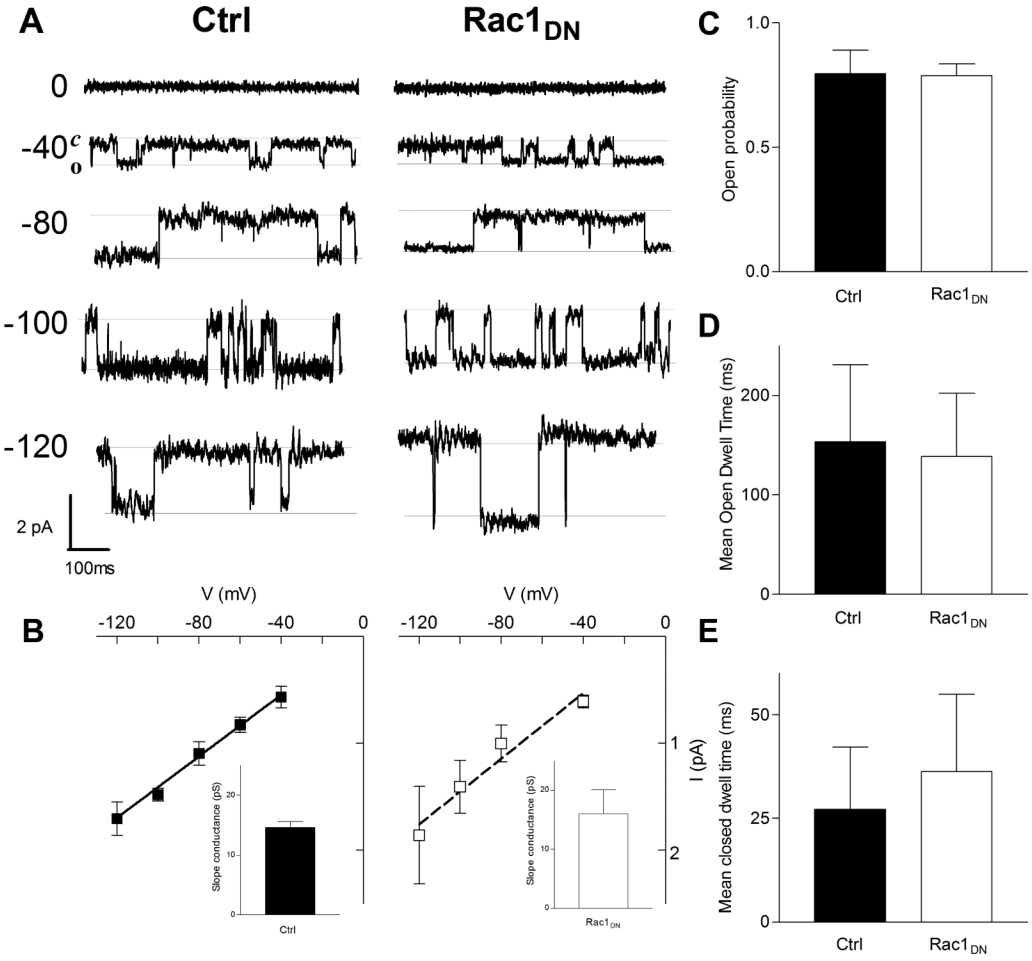

FIGURE 3. No Effect of $Rac1_{DN}$ On Kir2.1 Single-Channel Properties

A) Representative single-channel traces from control plasmid (Ctrl) or $Rac1_{DN}$ transfected cells in cell-attached patch clamp recordings at various voltages. The dashed line represents the closed state of the channel and the solid line represents the open state. *B*) Current-voltage relationship of single-channel currents from control (filled squares) and $Rac1_{DN}$ transfected cells (open squares). Lines represent linear fits to the data points; the solid line is the fit to control cells, the dashed line is the fit to $Rac1_{DN}$ transfected cells. Insets: Slope conductance calculated from linear fit to current amplitudes of individual cells using three or more data points. *C)* Open probability of Kir2.1 in control and $Rac1_{DN}$ transfected cells at –40 mV. *D)* Mean open and *E)* closed dwell times of control and $Rac1_{DN}$ transfected cells at –40 mV. Significance was tested using non-parametric t-tests. Data was obtained from 5-6 cells per condition.

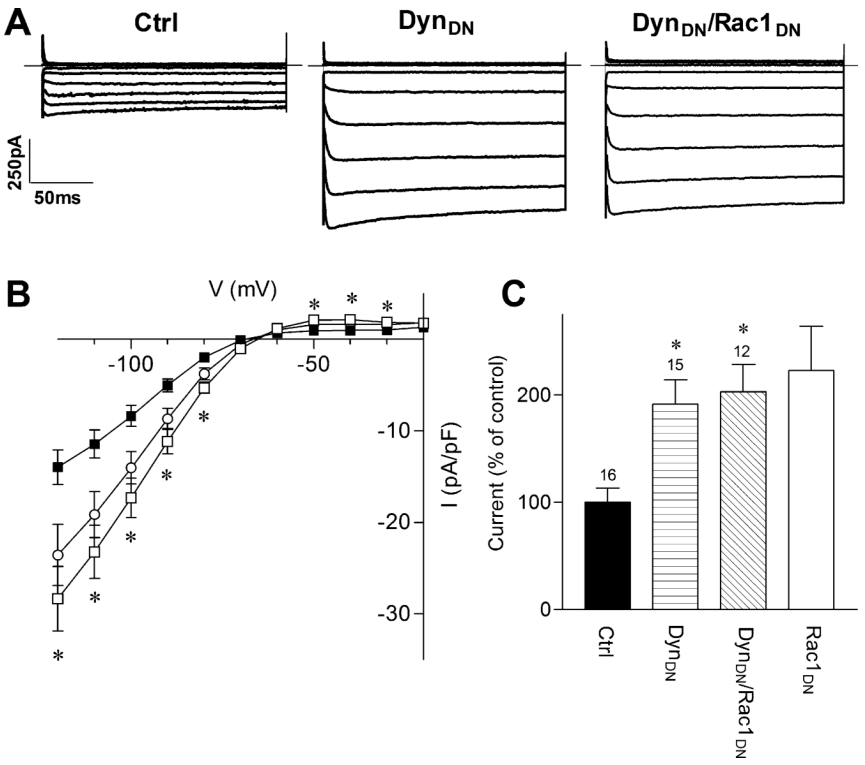

FIGURE 4. Dominant-Negative Dynamin Mimics and Occludes the Effect of Rac1DN on Kir2.1

A) Representative current traces from cells transfected with Kir2.1 cDNA and either a control plasmid (Ctrl), dominant-negative dynamin (Dyn_{DN}) or both Dyn_{DN} and $Rac1_{DN}$ cDNAs. Superimposed current traces are shown for 200 ms voltage steps from -120 to -20 mV in 10 mV increments from a holding potential of -60 mV. Scale bars: 50 ms and 250 pA. *B*) Current-voltage relationship for control (filled squares), Dyn_{DN} (open squares) and $Dyn_{DN}/Rac1_{DN}$ (open circles) transfected cells. *C*) Normalized current densities measured in control, Dyn_{DN}, and $Dyn_{DN}/Rac1_{DN}$ transfected cells at –100 mV. $Rac1_{DN}$ transfected cells from Fig. 2 are also included for comparison. Numbers above columns indicate number of cells in each condition. Asterisks denote statistically significantly different from control cells ($p < 0.05$), using a non-parametric Kruskil-Wallis ANOVA, followed by Dunn's multiple comparison post hoc test.

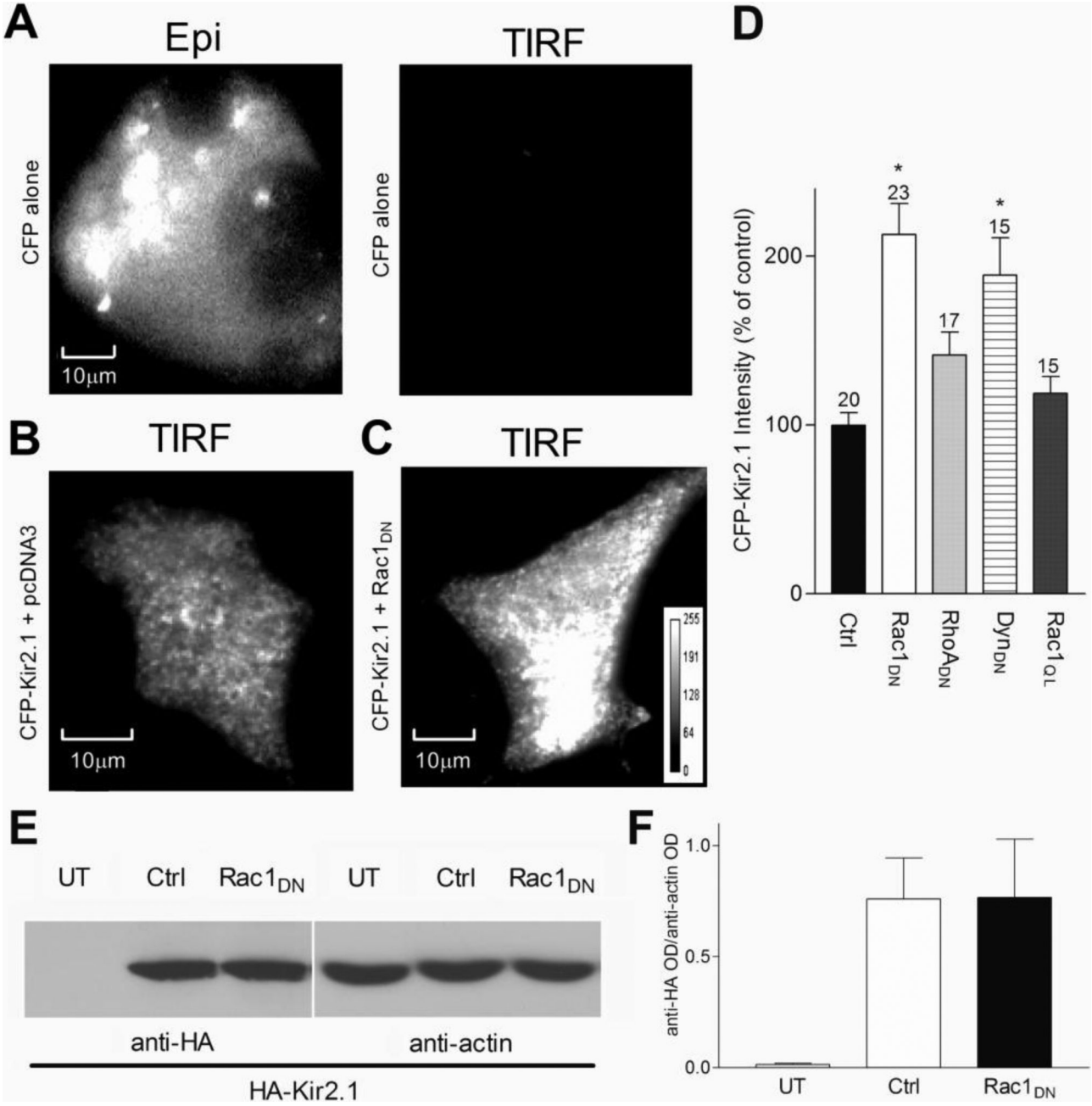

FIGURE 5. Rac1$_{DN}$ Increases Surface Expression of Kir2.1 Measured with TIRF Microscopy

Cells were transfected with the cDNA for a N-terminal CFP-tagged Kir2.1 in the absence or presence of Rac1$_{DN}$. *A)* Representative images from cells transfected with CFP cDNA viewed with epifluorescence (left: Epi) or TIRF (right) microscopy. All images have been scaled to the same intensity. *B-C)* Representative images from cells transfected with CFP-Kir2.1 cDNA and either a control plasmid (*B*) or Rac1$_{DN}$ (*C*) cDNA viewed with TIRF microscopy. Images have been scaled to the same intensity. Inset shows scale bar used to calibrate intensity. *D)* Quantitative analysis of CFP-Kir2.1 intensity under TIRF. Images were background-subtracted and analyzed using ImageJ software. Asterisks denote significance determined by non-parametric ANOVA and Dunn's post-hoc test (*, $p < 0.01$ and **, $p < 0.001$). *E)* Representative immnoblot for total HA-Kir2.1 protein in untransfected cells (UT) or cells transfected with

HA-Kir2.1 cDNA and either pcDNA3 (Ctrl) or $Rac1_{DN}$ cDNA. *Left:* Staining with anti-HA antibody. *Right:* Blots were stripped and reprobed with antibody against actin. *F)* Bar graph shows mean optical density (OD) measurements made using ImageJ. OD measurements for anti-HA bands were normalized to OD measurements for anti-actin bands to control for protein loading and expression levels (n=3). Asterisk indicates significance ($p > 0.05$) using unpaired Student's t-test.

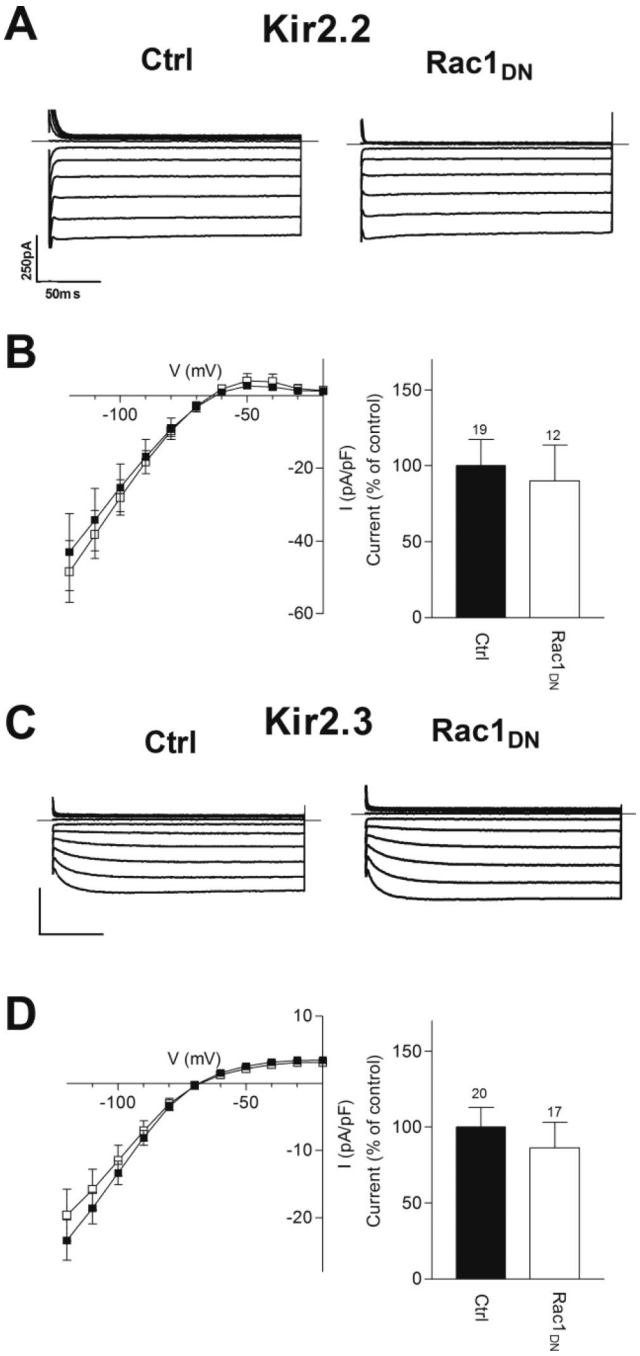

FIGURE 6. Kir2.2 and Kir2.3 Are Not Up-regulated by $Rac1_{DN}$

A&C) Representative current traces from cells transfected with *(A)* Kir2.2 or *(C)* Kir2.3 cDNA and either a control plasmid (Ctrl) or dominant-negative Rac1 ($Rac1_{DN}$) cDNA. Superimposed current traces are shown for 200 ms voltage steps from -120 to -20 mV in 10 mV increments from a holding potential of -60 mV. Scale bars: 50 ms and 250 pA. *B&D) Left:* Current-voltage relationship of Kir2.2 (B) or Kir2.3 (D) in control (filled squares) and $Rac1_{DN}$ (open squares) transfected cells. Right: Normalized current densities measured in control and $Rac1_{DN}$ transfected cells at –100 mV. Numbers above columns indicate number of cells in each condition. No significance was detected with non-parametric t-tests at <0.05.

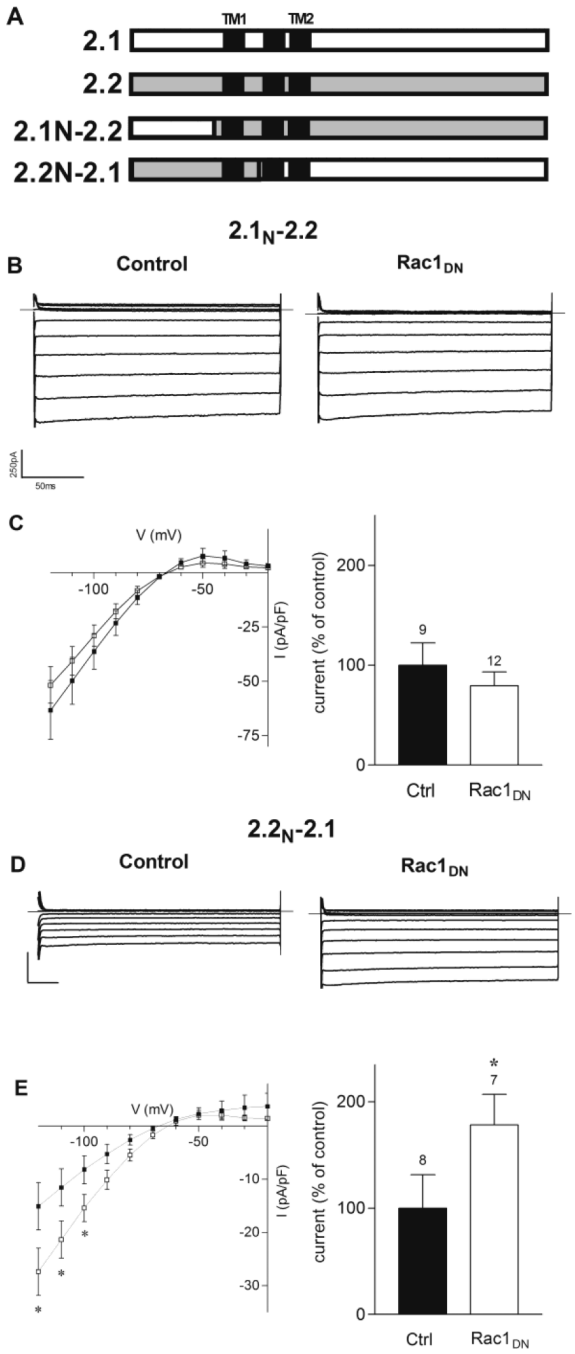

FIGURE 7. The C-terminal Domain of Kir2.1 Mediates the Potentiating Effect of $Rac1_{DN}$

A) Schematic of different Kir2.1/2.2 chimeric channels. 2.1_N-2.2, the N terminus of Kir2.1 fused to Kir2.2 at position 78. 2.2_N-2.1, Kir2.1 fused to Kir2.2 at position 121. *B)* Representative current traces from 2.1_N-2.2 transfected cells under control conditions or co-transfected with $Rac1_{DN}$. Superimposed current traces are shown for 200 ms voltage steps from -120 to -20 mV in 10 mV increments from a holding potential of -60 mV. *C) Left* Current-voltage traces of 2.1_N-2.2 under control conditions (filled squares) or co-transfected with $Rac1_{DN}$ (open squares). *Right:* Normalized current densities measured in 2.1_N-2.2 transfected cells under control conditions and co-transfected with $Rac1_{DN}$, at –100 mV. *D)* Representative current traces from 2.2_N-2.1 transfected cells under control conditions or co-transfected with

$Rac1_{DN}$. Scale bars: 50 ms and 250 pA. *E) Left:* Current-voltage traces of 2.2_N-2.1 under control conditions (filled squares) or co-transfected with $Rac1_{DN}$ (open squares). *Right:* Normalized current densities measured in 2.2_N-2.1 transfected cells under control conditions and co-transfected with $Rac1_{DN}$, at -100 mV. Numbers above columns indicate number of cells in each condition. Asterisks denote significance with non-parametric t-tests, ($p<0.05$).

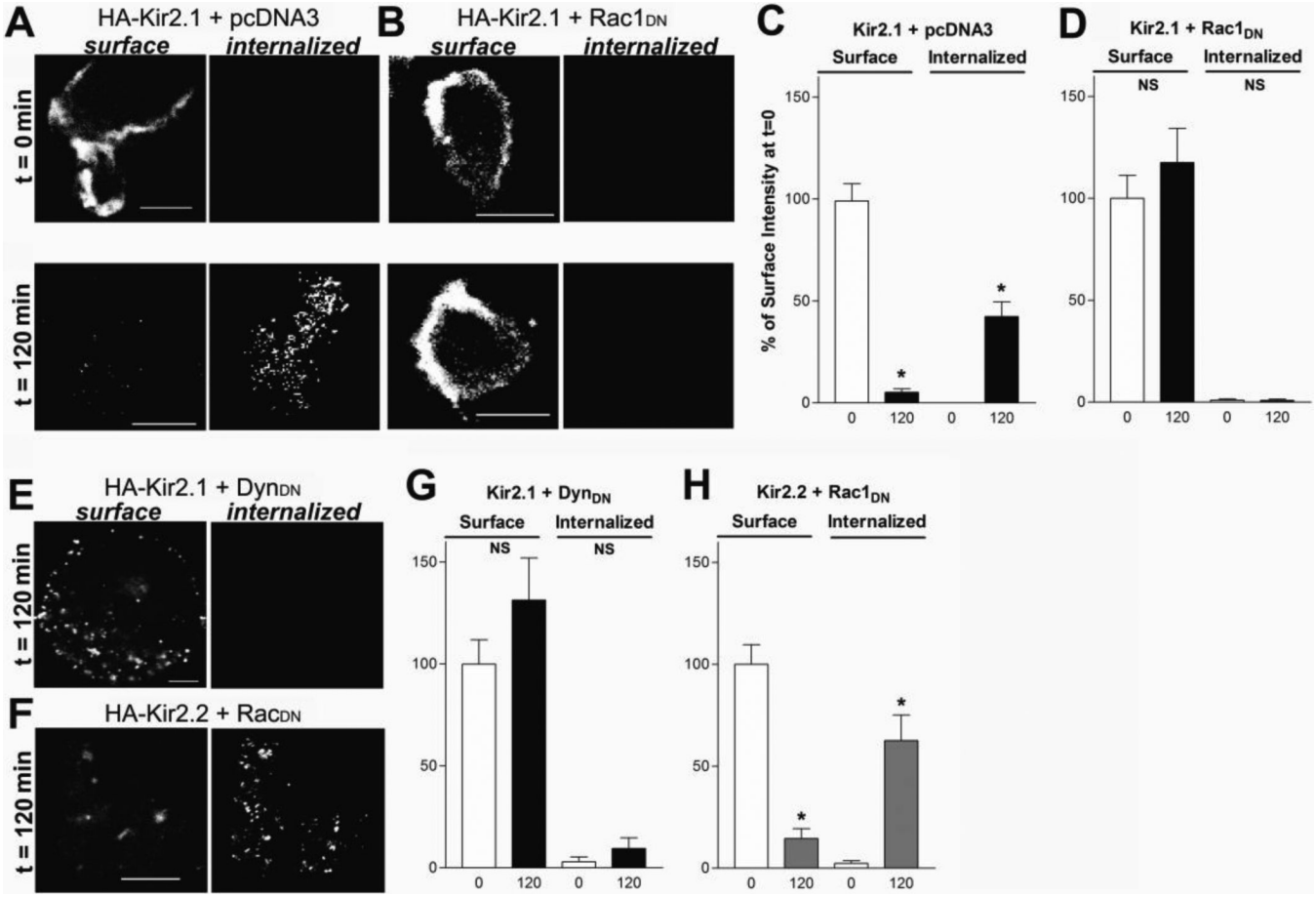

FIGURE 8. $Rac1_{DN}$ Inhibits Endocytosis of Kir2.1 Channels

A-B) Representative confocal images from cells expressing an extracellularly HA-tagged Kir2.1 channel cDNA and either *(A)* pcDNA3 or *(B)* $Rac1_{DN}$ cDNA Cells were incubated with anti-HA antibodies on ice 15min and returned to 37° C for 0 (t=0), or 120 (t=120) minutes. Cells were then incubated with Alexa-647 conjugated antibodies prior to permeabilization to label channels on the plasma membrane (*surface)*, and subsequently permeabilized and labed with Alexa-488 conjugated antibodies to visualize endocytosed channels (*internalized)*. $Rac1_{DN}$ co-expressing cells failed to show internalization of Kir2.1 even after 120 minutes. *D)* Representative confocal images from cells expressing Kir2.2 with an HA tag in the extracellular region coexpressed with $Rac1_{DN}$ after 120 minutes of incubation. Note the intense labeling of internalized channels. Scale bars: 10μm. *E-H)* Bar graphs show quantification of surface and internalized channel intensity after 0, 60 or 120 minute incubation periods for cells expressing HA-Kir2.1 and either *(E)* pcDNA3, *(F)* $Rac1_{DN}$ or (*G)* Dyn_{DN}, or (*H*) Kir2.2 and $Rac1_{DN}$. Intensity is expressed as a percent of the total surface intensity at time 0. Experiments were repeated three separate times. N=5-14 cells per condition.